Flexural Cracks in Fiber-Reinforced Concrete Beams with Fiber-Reinforced Polymer Reinforcing Bars

by Won K. Lee, Daniel C. Jansen, Kenneth B. Berlin, and Ian E. Cohen

Fiber-reinforced polymer (FRP) reinforcing bars have attracted considerable attention for applications where corrosion of steel reinforcement is problematic. Due to the generally low elastic modulus and poor bond characteristics of FRP as compared to steel reinforcing bars, the use of FRP results in larger crack widths under service loads. Fiber-reinforced concrete (FRC) is proposed for use with FRP to reduce crack widths. The work presented herein includes the results from 16 beams tested under four-point bending with either Grade 420 (Grade 60) steel or FRP reinforcing bars, and either plain concrete or FRC. A modified Gergely-Lutz model was applied to the measured crack widths to calculate bond coefficients that were used to quantify the effectiveness of FRC in reducing crack widths. In the beams with steel reinforcing bars, the FRC was found to have little influence on crack widths. In the beams with FRP reinforcing bars, the FRC was found to significantly reduce maximum crack widths.

Keywords: composites; crack widths; fiber-reinforced concrete; fiber-reinforced polymer; reinforced concrete.

INTRODUCTION

The corrosion of steel reinforcement is one of the most common causes of deterioration in reinforced concrete structures. Steel reinforcement embedded in concrete is ordinarily protected from corrosion by a passive oxide layer that forms on the surface of the reinforcement in the high pH environment provided by the cement paste. Corrosion can occur in the presence of moisture and oxygen, however, if the protective oxide layer is broken down. Corrosion is often initiated by chloride ions, which can penetrate the concrete to the level of the reinforcement and can lead to a breakdown of the protective oxide layer when the chloride ion concentration is sufficiently high. Structures susceptible to chloride-induced corrosion include those exposed to deicing salts (for example, highway bridges and parking structures) and those exposed to seawater (marine structures). Current methods of combating corrosion in reinforced concrete include protecting the reinforcing bar itself (for example, epoxy coatings and galvanized or stainless steel) or decreasing the permeability of concrete to prevent the ingress of chloride ions (through the use of silica fume, fly ash, and other pozzolans). The use of these methods, however, is inhibited by such factors as cost and questions of long-term effectiveness.

Recently, advanced composite materials have been applied to mitigate the problem of corrosion in reinforced concrete. One form of composite being studied is the composite reinforcing bar for use in place of traditional steel reinforcing bars. A number of recent studies has been performed using these composite bars as flexural reinforcement in reinforced concrete.[1-7] These composites, known commonly as fiber-reinforced polymers (FRPs), have high tensile strengths in comparison to steel and, more importantly, are resistant to corrosion. Additional benefits to the FRP bars are

their electromagnetic and radio transparency and their low weight compared to steel. However, FRP bars also have some characteristics that make them disadvantageous compared to steel. Most types of FRP have a low elastic modulus and a relatively poor bond to concrete as compared to steel bars. A direct result of these characteristics is larger crack widths and larger deflections under service loads as compared to beams reinforced similarly with steel. In addition, FRPs display linear elastic behavior in tension until failure and exhibit no yielding, making it difficult to design members to fail in a ductile fashion. Finally, concerns exist regarding the long-term durability of FRP bars (with respect to chemical, temperature, and other effects).[8]

To mitigate the problem of excessive crack widths arising from the use of FRP bars as flexural reinforcement, fiber-reinforced concrete (FRC) is proposed in place of plain concrete in FRP-reinforced beams. The addition of fibers has been shown to improve crack resistance in concrete.[9,10] The purpose of this study is to determine whether the use of FRC can improve the cracking response (as measured by maximum crack widths and number of cracks) of beams reinforced with FRP bars. In this study, plain and FRC beams with two types of FRP reinforcing bar and varying reinforcement ratios were tested under a four-point bending load, and the cracking response was measured in the constant-moment region of the beams. The cracking responses of the specimens were studied to quantify any improvements that came about as a result of the fiber reinforcement.

RESEARCH SIGNIFICANCE

The corrosion of reinforcing steel leads to the deterioration of many reinforced concrete structures. The use of composite materials such as FRPs can prevent corrosion deterioration, but their use can lead to excessive cracking due to their typically low elastic moduli and poor bond characteristics. The application of FRC to beams reinforced with FRP reinforcing bars is being investigated to determine the possible improvements to maximum crack widths. This is one of a limited number of experimental investigations that consider the use of a fiber-reinforced, cement-based matrix with FRP reinforcing bars. The research provides quantitative data on the crack width responses for plain and polypropylene FRC beams with both GFRP and CFRP reinforcing bars.

ACI member **Won K. Lee** *is a Structural Engineer at Forell/Elsesser Engineers, San Francisco, CA. He received his BS in civil engineering and his MS in structural engineering from Tufts University, Medford, MA, and his MS in mechanical engineering and PhD in structural engineering from Stanford University, Stanford, CA. His research interests include high-performance materials, sustainable building materials and design, finite element analysis, and seismic behavior of reinforced concrete structures.*

ACI member **Daniel C. Jansen** *is an Associate Professor at the California Polytechnic State University, San Luis Obispo, CA. He is a member of ACI Committees 363, High-Strength Concrete; 555, Concrete with Recycled Materials; and Joint ACI-ASCE Committee 446, Fracture Mechanics of Concrete. His research interests include high-strength concrete, high-performance materials, fracture and damage of concrete, and recycled materials.*

Kenneth B. Berlin *is the CEO at Blingfactor, LLC, and is pursuing his MBA from the UCLA Anderson School of Management, Los Angeles, CA. He received his BS in civil engineering from Tufts University and his MS in structural engineering from the University of Texas at Austin, Austin, TX.*

Ian E. Cohen *is an Attorney in New York City specializing in patent litigation. He received his BS in civil engineering and MS in structural engineering from Tufts University and his JD from Boston College Law School, Boston, MA.*
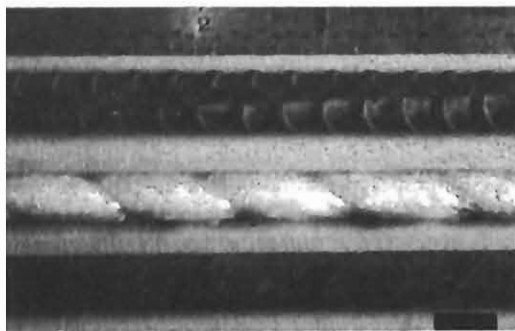
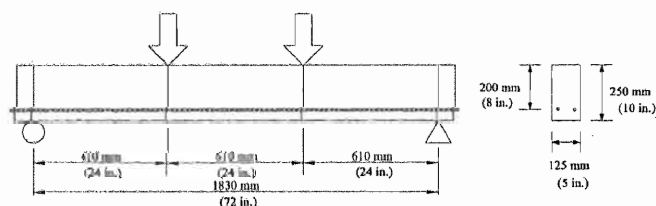*Fig. 1—Reinforcing bars (top to bottom: steel, GFRP, and FRP).*

Fig. 2—Specimen geometry and loading conditions.

EXPERIMENTAL INVESTIGATION
Materials
Reinforcing bars—Two types of FRP reinforcing bars are used in this investigation: glass FRP (GFRP) bars and carbon FRP (CFRP) bars. The GFRP bars are formed using the pultrusion method, and contain E-glass fibers in a vinylester resin matrix. The GFRP bars have a helically-wound fiber on the outside of the bar to produce surface deformations and are coated with a coarse silica sand to improve its bond to concrete. The CFRP bars are also formed using the pultrusion method, and contain carbon fibers in a thermosetting resin matrix. The CFRP bars have no surface coatings or deformations. The tensile stress-strain behavior of the FRP bars, typical of most types of FRP bars, is linear elastic until failure, with no ductility or yielding. The control beams contain conventional Grade 420 (Grade 60) steel reinforcing bars. The steel, GFRP, and CFRP reinforcing bars used in the study can be seen in Fig. 1, and the mechanical properties of the FRP bars are provided in Table 1. Although there appear

Table 1—Mechanical properties of reinforcing bars

Bar type	Bar size, metric (U.S.)	Nominal diameter, mm (in.)	Elastic modulus, GPa (ksi)	Yield strength, MPa (ksi)	Tensile strength, MPa (ksi)
GFRP	φ6 (No. 2)	6.4 (0.25)	37.8 (5490)	NA	507 (74)
GFRP	φ10 (No. 3)	9.5 (0.375)	43.3 (6280)	NA	769 (112)
GFRP	φ13 (No. 4)	12.7 (0.50)	45.6 (6610)	NA	690 (100)*
CFRP	φ6 (No. 2)	6.4 (0.25)	137.8 (20,000)	NA	2068 (300)*
CFRP	φ10 (No. 3)	9.5 (0.375)	132.3 (19,200)	NA	2068 (300)*
CFRP	φ13 (No. 4)	12.7 (0.50)	132.3 (19,200)	NA	2068 (300)*
Steel	φ10 (No. 3)	6.4 (0.25)	200.0 (29,000)	361 (52.4)	Not measured
Steel	φ13 (No. 4)	9.5 (0.375)	200.0 (29,000)	448 (65.0)	Not measured

*Data provided by manufacturer
Note: NA is not applicable.

to be surface deformations on the CFRP bar in Fig. 1, the apparent deformations are simply variations in color; the bar itself was quite smooth.

Concrete—Normal-strength concrete was used in this investigation. The concrete contained Type II portland cement and a Grade 100 ground, granulated blast-furnace slag at a 50% replacement of cement by weight. The maximum nominal size of the coarse aggregate was 9.5 mm (3/8 in.). The concrete had a water-cementitious material ratio (*w/cm*) of 0.46. The ratio of cement:slag:fine aggregate: coarse aggregate:water was 1:1:3.77:3.75:0.91. Air entrainment was provided to produce a concrete that would be representative of a mixture design used in a cold weather environment, where corrosion often occurs due to deicing salt exposure. An air-entraining admixture was used at a dosage of 82 mL/100 kg (1.3 oz/100 lb) of cementitious material for the plain concrete. The air content for plain concrete as measured using the pressure method was 7%. The target 28-day compressive strength of the concrete was 35 MPa (5 ksi).

The FRC used in this investigation contained crimped, polypropylene fibers at a fiber volume fraction of 1%. The polypropylene fibers had a tensile strength of 540 MPa (78 ksi) and an elastic modulus of 9.5 GPa (1378 ksi). The fibers were 40 mm (1.56 in.) in length with an aspect ratio of 90. The FRC had the same mixture proportions as the plain concrete, with the exception that a Type F, high-range water-reducing admixture was used to provide adequate workability given the presence of the fibers. A high-range water-reducing admixture was used at a dosage of 240 mL/100 kg (3.7 oz/100 lb) of cementitious material. An air-entraining admixture was used at the same proportions as the plain concrete mixture, with a resulting air content of approximately 10%.

Specimens
The reinforced concrete beam specimens were rectangular in cross section, with a width of 125 mm (5 in.) and a height of 250 mm (10 in.). Each reinforced beam specimen contained two reinforcing bars placed in a single layer at a depth of 200 mm (8 in.). Specimen geometry and reinforcement layout details can be seen in Fig. 2. The reinforcing bar types tested were GFRP, CFRP, and Grade 420 (Grade 60) steel using bar sizes of either φ6 (No. 2), φ10 (No. 3), or φ13 (No. 4). A total of 16 beams were tested and are listed in Table 2 with their respective reinforcement ratios. The beams with φ6

Table 2—Test specimens

Specimen	Reinforcing bar type	Bar size, metric (U.S.)	Concrete type	Companion cylinder strength, MPa (psi)	Modulus of rupture, MPa (psi)	Reinforcing ratio ρ, %	Balanced reinforcing ratio ρ_b,* %
G2N0	GFRP	φ6 (No. 2)	Plain	43 (6180)	5.6 (810)	0.25	0.96
G3N0	GFRP	φ10 (No. 3)	Plain	39 (5720)	6.1 (890)	0.55	0.48
G4N0	GFRP	φ13 (No. 4)	Plain	39 (5720)	5.4 (780)	0.98	0.61
G2P1	GFRP	φ6 (No. 2)	FRC	31 (4490)	5.2 (750)	0.25	0.78
G3P1	GFRP	φ10 (No. 3)	FRC	33 (4810)	5.2 (750)	0.55	0.43
G4P1	GFRP	φ13 (No. 4)	FRC	30 (4300)	5.0 (720)	0.98	0.51
C2N0	CFRP	φ6 (No. 2)	Plain	39 (5720)	5.5 (790)	0.25	0.43
C3N0	CFRP	φ10 (No. 3)	Plain	43 (6170)	5.5 (790)	0.55	0.48
C4N0	CFRP	φ13 (No. 4)	Plain	42 (6040)	5.7 (820)	0.98	0.45
C2P1	CFRP	φ6 (No. 2)	FRC	35 (5010)	5.2 (750)	0.25	0.39
C3P1	CFRP	φ10 (No. 3)	FRC	31 (4490)	5.2 (750)	0.55	0.39
C4P1	CFRP	φ13 (No. 4)	FRC	33 (4760)	5.0 (720)	0.98	0.39
S3N0	Steel	φ10 (No. 3)	Plain	38 (5560)	5.6 (810)	0.55	3.60
S4N0	Steel	φ13 (No. 4)	Plain	51 (7460)	6.7 (970)	0.98	4.23
S3P1	Steel	φ10 (No. 3)	FRC	29 (4260)	7.8 (690)	0.55	2.99
S4P1	Steel	φ13 (No. 4)	FRC	36 (5220)	4.9 (710)	0.98	3.45

*Computed using experimentally measured values where available.

(No. 2) and φ10 (No. 3) bars were under-reinforced beams, while the beams with φ13 (No. 4) beams were over-reinforced.

The beams were cast using a standard laboratory drum mixer. Two reinforced concrete beams, nine 100 x 200 mm (4 x 8 in.) compression cylinders, and three 100 x 100 x 355 mm (4 x 4 x 14 in.) modulus of rupture prisms were cast at the same time. The cylinders were used to measure compressive strength and static modulus of elasticity. Each reinforced beam was filled in three layers, and consolidation was performed with the use of an internal vibrator. All specimens were cured at room temperature (16 to 27°C [60.8 to 80.6°F]) for 24 hours. After 24 hours, the specimens were removed from their forms. The reinforced beams were wrapped in wet burlap, covered in plastic, and allowed to cure for 14 days at room temperature. After 14 days, the plastic and wet burlap were removed and the reinforced beams were allowed to cure in the ambient environment until testing. Specimens were tested at an age between 27 and 31 days. Six of the compression cylinders were placed in a 100% relative humidity environment at 23°C (73.4°F) after demolding for curing until testing at an age of 28 days as per ASTM C39 standards. The remaining three cylinders (referred to as companion cylinders) and the three modulus of rupture prisms were kept with the reinforced concrete beam specimens after demolding to cure under the same conditions. These specimens were tested at the same time as the reinforced concrete beams to better represent the actual mechanical properties of the concrete in the beam.

Testing configuration

The beams were simply supported and subjected to a four-point bending load, as shown in Fig. 2. The beams contained no compression reinforcement and no internal shear reinforcement. The beams were tested in a screw-driven testing machine with a 1.33 MN (300 kip) load capacity. A reinforced beam specimen in the testing machine is shown in Fig. 3. The shear reinforcement consisted of externally applied steel stirrups. Ten external, 19 mm (3/4 in.) diameter stirrups were applied at a spacing of roughly 50 mm (2 in.) on the two outer spans to prevent shear failure. The stirrups were attached and tightened prior to testing. External stirrups
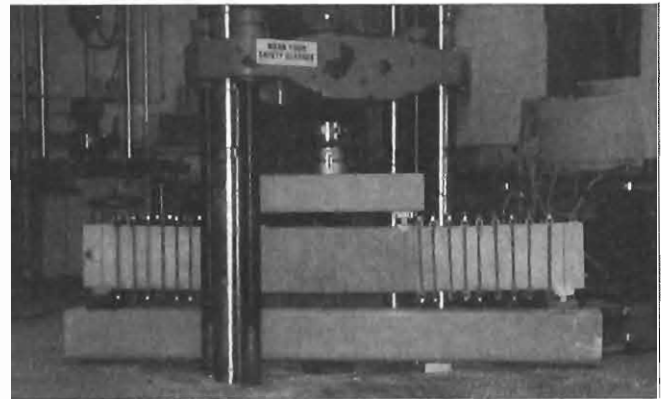

Fig. 3—Photograph of beam being tested.

were used rather than internal stirrups because of the fact that they could be reused for each beam specimen, thus conserving materials and time for bending the reinforcing bars. Although the confining effect of the external stirrups was not as great as that of internal stirrups, it was not expected to significantly influence the testing results. Loading was applied in a quasi-static manner, with a constant testing machine crosshead displacement rate of 0.5 mm/minute (0.02 in./minute). For a full description of the testing procedures, refer to Lee.[11]

Digital image analysis for crack width measurement

A digital image analysis system was used to measure the formation and growth of cracks in a specimen during testing. The digital image analysis system is a nondestructive method of data acquisition that does not require the direct attachment of any instrumentation to the specimen. Digital image analysis is essentially used as a method of measuring relative displacements across the surface of a specimen. The system requires the capture of high-resolution digital images of the face of a specimen throughout the testing.

The principle upon which the digital image analysis is based is the matching of image subsets between two different images, as shown in Fig. 4. The first image, or the
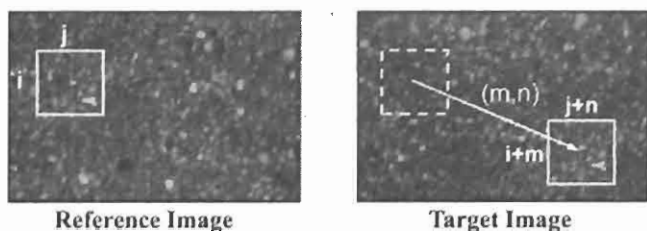
Reference Image   Target Image

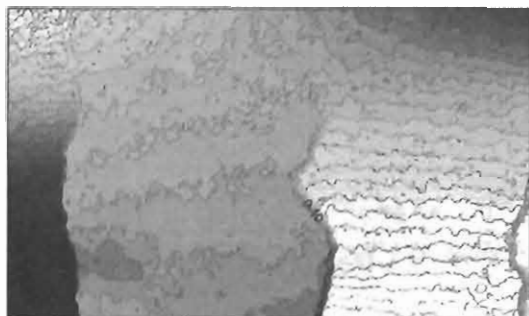*Fig. 4—Image subset matching for digital image analysis.*

Fig. 5—Example contour plot of horizontal displacements from processed digital image (corresponds to Fig. 13 for Specimen G4N0).
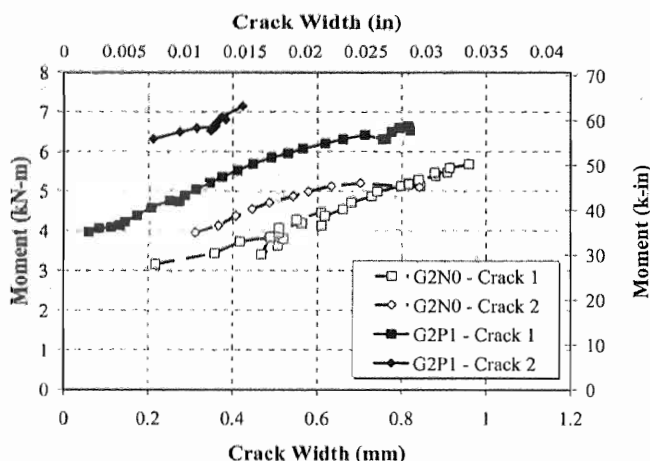

Fig. 6—Moment versus crack widths in $\phi6$ (No. 2) GFRP-reinforced beams.

reference image, is of the undeformed specimen (that is, prior to the application of any load). The second image, or the target image, is of the deformed specimen at some point during loading. The digital image analysis system determines the change in location of a small, square subset region of the image, or sub-image, between the reference image and the target image. This change in location is given in terms of relative horizontal and vertical displacements. For any given sub-image on the reference image, the target image is scanned until that same sub-image is located. Once the new location of the sub-image is found, the vector displacement (m, n) is determined. Matching of image subsets is then performed at a regularly spaced grid of nodes (each node being at the center of a sub-image) across the entire image. The specimen surfaces to be photographed are sprayed with a speckle pattern of various shades of paint (as shown in Fig. 4) to provide distinct patterns that are distinguishable for matching by the digital image analysis software.

The processing of the vector displacements for any given target image can provide surface displacement maps and allows for the measurement of cracks throughout the entire face of the specimen. In this research, a high resolution camera was used to capture images of one face of the beam in the constant-moment region at regularly spaced time intervals. Each image was then processed to produce contour plots of vertical and horizontal displacements, as well as measurements of crack widths at multiple heights in the cross section for all cracks. An example contour plot of horizontal surface displacements from a processed image is shown in Fig. 5. Three cracks are visible in the contour plot, and their widths can be measured to a high precision. Based on previous experience, the system has been shown to have an average resolution slightly better than 0.008 mm (0.0003 in.). Further details on the digital image analysis system and processing of images to determine crack widths can be found in Lee[11] or Jansen et al.[12]

EXPERIMENTAL RESULTS AND DISCUSSION

The beam testing results with regard to failure modes, load-deflection response, and moment-curvature response are not presented in this paper, as the primary focus is on the cracking behavior. Full details of the beam testing results can be found in Lee.[11] The modulus of rupture and companion cylinder compressive strength values are given in Table 2. The compressive strength of the FRC was found, on average, to be approximately 23% lower than the plain concrete. The lower compressive strength is likely due to the increased air content of the FRC concrete mixtures.

To compare the cracking behavior between the beam specimens, plots are made of the moment versus the crack width. The crack widths are measured within the constant-moment region of the beam. The digital image analysis system allowed for the measurement of the crack widths at any height of interest in the specimen. The crack widths are taken at the height of the reinforcing bars, and all individual cracks are shown in the plots.

Crack widths in GFRP-reinforced beams

For beams reinforced with GFRP bars, the polypropylene fibers improved the cracking behavior of the beams with respect to the size of crack widths that were observed. Shown in Fig. 6 is the moment versus crack width plot comparing the two specimens reinforced with $\phi6$ (No. 2) GFRP bars (G2N0 and G2P1). The number of cracks present in both beams is the same, as two cracks had formed in both specimens; however, the widths of the cracks in the beam with FRC are significantly smaller than in the beam without fiber reinforcement. Comparing the two beams at a moment of 5 kN-m (44 kip-in.), the maximum crack width in Specimen G2N0 is approximately 0.75 mm (0.030 in.), whereas the maximum crack width in Specimen G2P1 is only 0.30 mm (0.012 in.).

For Specimens G4N0 and G4P1 ($\phi13$ [No. 4] GFRP bars), which were over-reinforced beams, the fiber reinforcement greatly improves the cracking response that was observed, as shown in Fig. 7. In Specimen G4N0, only three cracks formed, all within a short time span of each other. As loading continued, these three cracks continued to grow without the formation of additional cracks. In contrast, Specimen G4P1 saw the formation of several additional intermediate cracks following the formation of the first cracks. The formation of new cracks was made possible by the presence of the fibers. The ability of the fibers to carry tensile stress at the locations
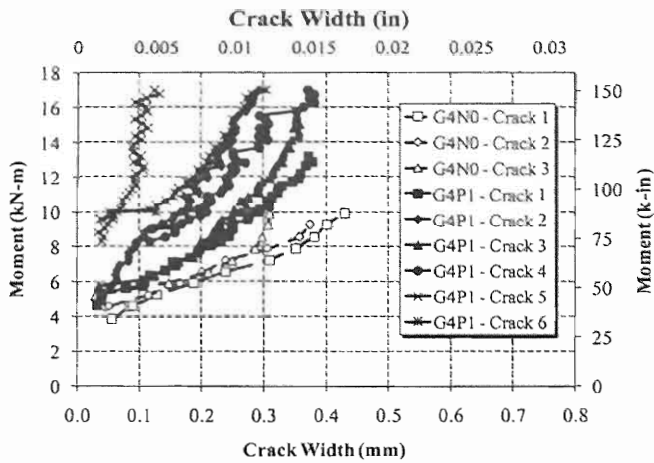
Fig. 7—Moment versus crack widths in $\phi13$ (No. 4) GFRP-reinforced beams.

of the cracks prevented the localization of the cracking to a degree, which allowed for the formation of successive, intermediate cracks in the specimen. This effect was pronounced in the two over-reinforced specimens, as the number of cracks observed in Specimen G4P1 was double the number observed in Specimen G4N0. The final crack patterns for Specimens G4N0 and G4P1 are shown in Fig. 8.

Crack widths in CFRP-reinforced beams

As with the GFRP-reinforced specimens, the presence of the polypropylene fibers significantly improved the cracking behavior of the CFRP-reinforced specimens. The same trends are seen as in the GFRP-reinforced specimens, where the beams with lower reinforcement ratios saw reductions in crack widths but not the number of cracks, whereas the over-reinforced beams saw reductions in crack widths and an increase in the number of cracks that formed. Shown in Fig. 9 is the moment versus crack width plot for Specimens C2N0 and C2P1 ($\phi6$ [No. 2] CFRP bars). The difference in the maximum crack width observed between the two beams is substantial. At a moment of 10 kN-m (89 k-in.), the maximum crack width seen in Specimen C2N0 is approximately 1.1 mm (0.043 in.), whereas the maximum crack width seen in Specimen C2P1 is only 0.6 mm (0.024 in.).

The beams that experience the greatest benefit to the cracking response with the addition of fiber reinforcement are the two specimens with $\phi13$ (No. 4) CFRP reinforcing bars (Specimens C4N0 and C4P1). Like the two over-reinforced beams with GFRP bars, the number of cracks increased with the presence of fibers. It was the crack widths, however, that were most affected by the presence of the fibers. The crack widths in Specimen C4N0 were considerably higher than in Specimen C4P1. The moment versus crack width plot for these two beams was shown in Fig. 10. At a moment of 15 kN-m (133 k-in.), there was a large difference in the maximum crack width observed in the two beams. The maximum crack width in Specimen C4N0 was approximately 1.0 mm (0.039 in.), in comparison with a maximum crack width in Specimen C4P1 of approximately 0.3 mm (0.012 in.). The final crack patterns for Specimens C4N0 and C4P1 are shown in Fig. 11. The reduction in crack widths with the presence of the polypropylene fibers for beams with both types of FRP bars is similar to what has been found in another study.[13]
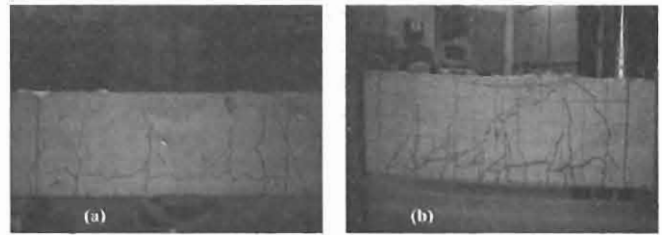

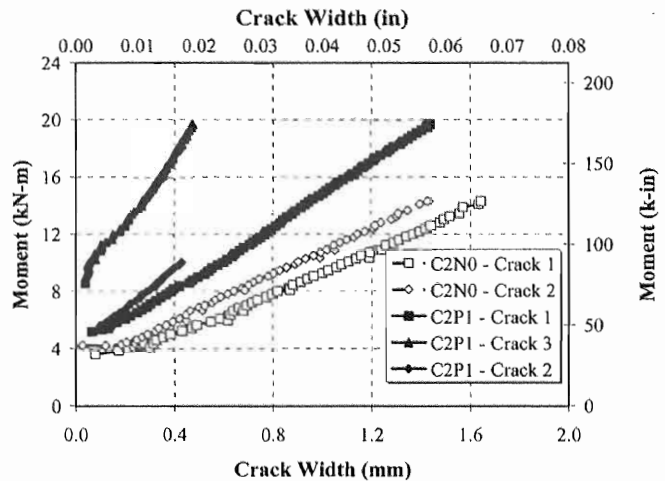Fig. 8—Final crack patterns for beams: (a) Specimen G4N0; and (b) Specimen G4P1.

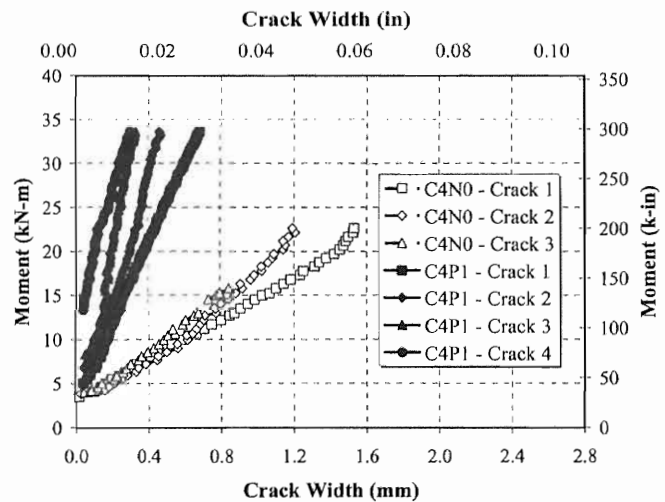Fig. 9—Moment versus crack widths in $\phi6$ (No. 2) CFRP-reinforced beams.

Fig. 10—Moment versus crack widths in $\phi13$ (No. 4) CFRP-reinforced beams.

Crack widths in steel-reinforced beams

The presence of fiber reinforcement does not significantly affect the cracking response of beams reinforced with steel bars. The number and width of cracks observed in specimens with steel bars does not vary between beams with plain concrete and those with FRC. The plots of moment versus crack width for Specimens S3N0 and S3P1 can be seen in Fig. 12. While it appears that there are two cracks in Specimen S3S1 and only one crack in Specimen S3N0, a second crack had in fact formed in Specimen S3N0 but was outside the
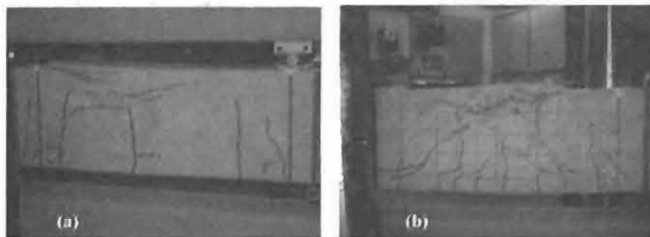
Fig. 11—Final crack patterns for beams: (a) Specimen C4N0; and (b) Specimen C4P1.
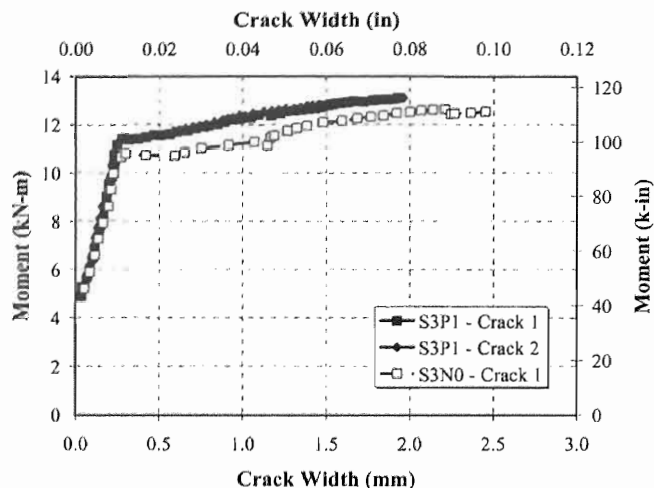

Fig. 12—Moment versus crack widths in $\phi10$ (No. 3) steel-reinforced beams.

range of the viewing area of the digital image analysis (that is, it was not within the area of the beam captured by the digital photograph) and could therefore not be measured. The fibers had no effect on the crack widths while the steel remained elastic, which was the region of importance in design considerations. Whereas the crack widths slightly decreased with the use of fibers after the steel began to yield, the actual width of the cracks after that point became less important. The yielding of steel in a reinforced concrete structural element corresponds to the overload of that member, and serviceability considerations lose importance as compared to safety considerations. Similar behavior is seen in Specimens S4N0 and S4P1.

The fact that the fibers do not significantly affect the cracking response of the specimens is likely due to the high elastic modulus and better bond characteristics of the steel reinforcing bars, in addition to the low modulus of the fibers in comparison to the reinforcing bars. A higher volume fraction of fibers or the use of stiffer fibers (for example, steel fibers) may have led to a more pronounced effect on the cracking response of the steel-reinforced beams.

CRACK WIDTH MODELING
Use of modified Gergely-Lutz equation
ACI Committee 440 has modified the Gergely-Lutz equation for predicting crack widths for use with FRP-reinforced concrete members.[14] The original Gergely-Lutz equation was an empirical equation that was developed based on data from numerous steel-reinforced concrete specimens.[15] The suggested modifications are based on theoretical and experimental studies performed by several researchers[16-19] on FRP-reinforced concrete members and are implemented to incorporate the effects of the differing bond and mechanical properties of FRP reinforcement compared to steel reinforcement. Other recent research has led to further proposed modifications of the ACI 440 equation[20]; however, only the current ACI 440 equation is considered herein.

The Gergely-Lutz equation for FRP-reinforced members is modified from the original equation by a corrective coefficient that accounts for the differences in bond characteristics between steel reinforcement and FRP reinforcement. This modified Gergely-Lutz equation is shown in Eq. (1)

$$w = \frac{2.2}{E_f}\gamma k_b f_f \sqrt[3]{d_c A_r} \text{ mm, MPa} \qquad (1)$$

Plots of the moment versus the crack width are created for all reinforced concrete beam specimens tested. To calculate the crack width from the applied moment using the Gergely-Lutz equation, it is necessary to express the stress in the reinforcement in terms of the moment. This relationship is shown in Eq. (2), and follows from a cracked section analysis.

$$f_f = E_f \varepsilon_f = \frac{E_f}{E_c} \cdot \frac{d - \bar{y}_{cr}}{I_{cr}} \cdot M \qquad (2)$$

As the stress can now be represented as a function of the moment, the modified Gergely-Lutz equation can now be used to plot the moment versus the crack width. The substitution of Eq. (2) into Eq. (1) yields the modified Gergely-Lutz equation expressed as a function of the applied moment, which can be seen in Eq. (3)

$$w = \frac{2.2}{E_c} \cdot \frac{d - \bar{y}_{cr}}{I_{cr}}\gamma k_b M \sqrt[3]{d_c A_r} \qquad (3)$$

Calculating crack width at height of reinforcement
The crack widths at the height of the reinforcing bars on the face of the specimen are determined from the digital image analysis. The Gergely-Lutz equation is used for calculating the maximum crack width at the extreme tensile face of the specimen. To use the Gergely-Lutz equation for comparison with the data, the equation is used with the value of γ set equal to 1. The value of γ is equal to the ratio of the distance from the neutral axis to the tensile face of the specimen (where the crack width is to be calculated) and the distance from the neutral axis to the centroid of the tensile reinforcement. Therefore, if the crack widths vary linearly throughout the height of the cross section, the crack width at the height of the reinforcing bars can be calculated using a γ value of 1.

The use of the Gergely-Lutz equation for calculating the crack width at the height of the reinforcing bars is dependent on the assumption that the crack widths vary linearly with height. This assumption is found to be valid based on the results from the digital image analysis. The digital image analysis allows for the measurement of crack widths at multiple heights in the specimen and, therefore, the variation of crack width with height can be easily seen. In all cases, the crack widths are indeed found to vary linearly with height. Figure 13 shows the variation of crack width with height for Specimen G4N0 for the image shown in Fig. 5.

Table 3—Calculated bond coefficients

| Reinforcing bar type | Reinforcing bar size | Corrective bond coefficient, k_b | | $k_{b,FRC}/k_{b,Plain}$ |
		Plain concrete	FRC	
Steel	3	1.02	1.01	0.99
	4	0.73	0.61	0.84
GFRP	2	1.57	0.67	0.42
	3	1.97	0.84	0.43
	4	1.04	0.57	0.55
CFRP	2	1.74	0.92	0.53
	3	1.55	0.95	0.61
	4	2.98	0.76	0.26

At the time when this image was taken, it can be seen that two fairly large cracks have formed in the specimen. The behavior seen is typical of the behavior seen in all of the specimens. The crack widths vary linearly regardless of the load or the number of cracks present. This observation allows for the Gergely-Lutz equation with a γ value of 1 to be used to calculate the crack widths at the height of the reinforcement.

The modified Gergely-Lutz equation was compared with the experimentally observed crack width behavior in the beams. The observed behavior, however, was fundamentally different than what was predicted by the Gergely-Lutz equation. The Gergely-Lutz equation for predicting crack widths is a linear equation (with a slope depending on the material and section properties) that passes through the origin. The observed response, however, was that the plot of moment (which is related to the stress in the reinforcement) versus crack width will not, if extrapolated backwards, pass through the origin. Intuitively, the plot would not be expected to pass through zero, as a crack does not form immediately with application of moment (neglecting preexisting microcracks), and will only form when the tensile strength of the concrete has been reached. This behavior was observed in all specimens tested, with all plots intercepting the ordinate at a point that was not the origin.

To account for the differences seen in the cracking behavior between specimens and with respect to the Gergely-Lutz equation, a linear regression was performed on the data with the line forced through the experimentally measured cracking moment of the beam. It was at the cracking moment where the crack first formed and began to increase in width with increasing moment. A modification to the Gergely-Lutz equation was used to allow the equation for maximum crack width to pass through a point on the y-axis equal to the cracking moment, rather than forcing it to pass through the origin. The modification to the Gergely-Lutz equation is given in Eq. (4)

$$w = \frac{2.2}{E_c} \cdot \frac{d - \bar{y}_{cr}}{I_{cr}} \gamma k_b (M - M_{cr}) \sqrt[3]{d_c A_r} \quad M > M_{cr} \quad (4)$$

Linear regressions are then performed for all specimens with the lines forced through the y-axis at a moment equal to the cracking moment. For example, the moment versus maximum crack width and the best-fit linear regressions for Specimens C4N0 and C4P1 are shown in Fig. 14.
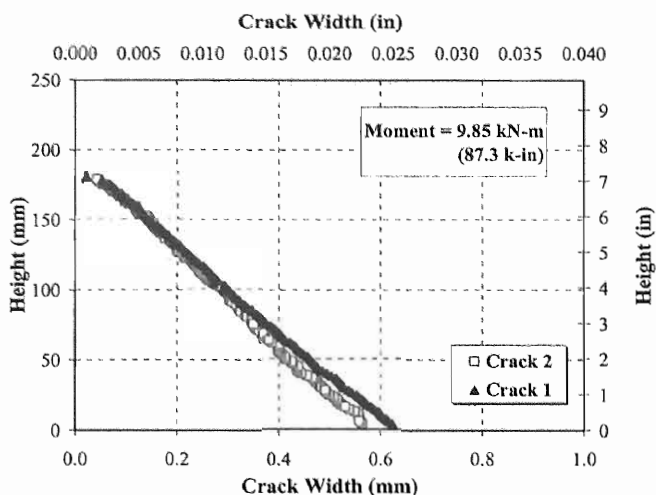

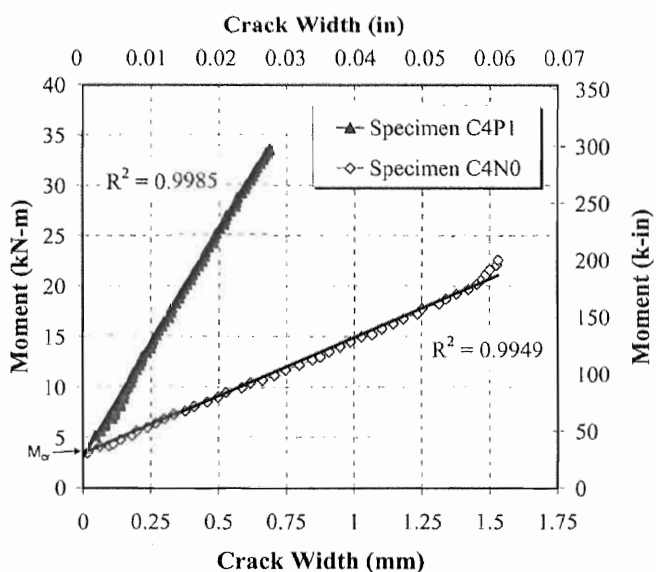Fig. 13—Crack width versus height (Specimen G4N0).

Fig. 14—Moment versus maximum crack width for φ13 (No. 4) CFRP-reinforced beams.

Corrective bond coefficients

The slope of the best-fit linear regressions are used to back-calculate the corrective bond coefficient k_b using Eq. (4). The bond coefficients are calculated for all specimens tested, and a summary of the results is given in Table 3. It should be noted that the following comments are based on the results from the testing of a single beam in each case. Further experimental studies should be conducted to generate additional data and thus allow for more conclusive results.

For a given reinforcing bar type, no clear correlation between the bond coefficient and the bar size/reinforcement ratio was observed, in the sense that the bond coefficients do not monotonically increase or decrease with increasing bar size/reinforcement ratio. The value of the bond coefficient for FRC beams, however, was consistently smaller than the value for plain concrete beams. While it was difficult to make any strong conclusions regarding the effect of bar size/reinforcement ratio on the bond coefficient, it was clear that the addition of polypropylene fibers to the concrete consistently leads to reduced values when FRP reinforcing bars are used.

The bond coefficients found for steel bars with plain concrete were close to 1, as expected, because the original Gergely-Lutz equation was based on the use of steel-reinforced concrete. A reduction in the bond coefficient from a value of 1 would, in the context of the Gergely-Lutz equation, mean improved bond characteristics of the reinforcing bar in comparison to steel. In a more general sense, however, it would mean that there would be a decrease seen in the maximum crack widths observed. The use of fiber reinforcement has been shown to improve the bond characteristics of reinforcing bars to concrete.[21-23] Therefore, the decrease in the bond coefficient signifies both improved bond between concrete and reinforcing bar, as well as an overall reduction in crack widths due to bridging effects of the fibers.

There was little reduction in the value of the corrective bond coefficient with the use of FRC in the steel-reinforced specimens, as the value of k_b was reduced by only 1% for the beam with $\phi10$ (No. 3) bars and by approximately 16% for the beam with $\phi13$ (No. 4) bars. This was not a large reduction, and was consistent with the observed cracking response, as the crack widths were seen to be nominally unaffected by the presence of the polypropylene fibers.

The bond coefficients found for the three GFRP beams were larger than 1, meaning that the GFRP bars had bond characteristics worse than that of steel, despite the fact that the bars had lugs and a coarse sand-epoxy coating meant to improve the bond characteristics. The bond coefficient values are shown in Table 3. Research has shown that the bond between FRP bars and concrete is highly dependent on and can be greatly improved by the lug geometry and resin properties.[24,25] Studies on various GFRP bars from different manufacturers have shown bond coefficients ranging from 0.71 to 1.83, meaning that the bars can have bond characteristics superior to or inferior to steel.[14] The bond coefficient for the GFRP-reinforced beams with FRC were reduced by approximately 57% for the $\phi6$ (No. 2) and $\phi10$ (No. 3) beams and by approximately 45% for the $\phi13$ (No. 4) beam as compared to their counterpart beams with plain concrete. The significant decrease in the maximum crack widths observed is a result of this considerable decrease in the bond coefficient.

The bond coefficients for the CFRP-reinforced beams with plain concrete were also greater than 1. The bond coefficients are presented in Table 3. The values are much higher than those found for the beams with steel reinforcement, which indicates a significant reduction in the bond quality of the CFRP reinforcing bars. The CFRP bars used in this study were very smooth, with no physical deformations or coatings to improve its bond to concrete. The high value of the bond coefficient that was found was not unexpected.

Like the GFRP-reinforced specimens, the addition of polypropylene fibers to the concrete leads to a large reduction in the bond coefficient. The bond coefficient is reduced by approximately 47, 39, and 74% for the beams with $\phi6$ (No. 2), $\phi10$ (No. 3), and $\phi13$ (No. 4) bars, respectively. The reduction in maximum crack widths observed is the most pronounced in the specimens with the CFRP bars, which are smooth and have no deformations. The presence of fibers has a greater effect on reducing crack widths when used with reinforcing bars with poor bond characteristics.

CONCLUSIONS
The cracking behavior of plain and polypropylene FRC beams with either steel, GFRP, or CFRP reinforcing bars was measured using a digital imaging system. The following conclusions can be drawn from the results of the experimental investigation:

1. The addition of polypropylene fibers to the concrete improves the cracking behavior (reduced crack widths and spacing) of beams reinforced with FRP bars, with more improvement seen in beams with CFRP reinforcing bars than in beams with GFRP reinforcing bars.

2. The addition of polypropylene fibers to the concrete does not significantly improve the preyield cracking behavior of beams reinforced with steel bars.

3. A modification to the Gergely-Lutz equation given by ACI Committee 440 for predicting crack widths in FRP-reinforced beams is implemented and was used to calculate bond coefficients for FRP-reinforced beams with plain concrete and FRC. The bond coefficients were used as a proxy to quantify the improvements to the crack width response of the beams, where reduced bond coefficients signified reductions in maximum crack width. The use of FRC was found to reduce the bond coefficient on the order of 45 to 55% for the GFRP-reinforced beams, 45 to 75% for the CFRP-reinforced beams, and 1 to 15% for the steel-reinforced beams. Based on the data found in this set of tests, no clear correlation between bond coefficient and bar size/reinforcement ratio was found.

NOTATION
A_r = concrete area surrounding one tension bar equal to total effective tension area of concrete surrounding reinforcement and having same centroid, divided by number of bars
d = depth to centroid of tension reinforcement
d_c = thickness of concrete cover measured from tension face to center of bar closest to that face
E_c = elastic modulus of concrete
E_f = elastic modulus of FRP reinforcement
f_f = stress in FRP reinforcement
I_{cr} = moment of inertia of cracked section
k_b = corrective bond coefficient
M = applied moment
M_{cr} = cracking moment
w = crack width
$\bar{y}_{cr}$ = depth to centroid of cracked section
ε_f = strain in FRP reinforcement
γ = ratio of distance from tension face to neutral axis to distance from centroid of reinforcement to neutral axis

REFERENCES
1. Nanni, A., "Flexural Behavior and Design of RC Members Using FRP Reinforcement," Journal of Structural Engineering, V. 119, No. 11, 1993, pp. 3344-3359.
2. Nanni, A.,"North American Design Guidelines for Concrete Reinforcement and Strengthening Using FRP: Principles, Applications and Unresolved Issues," Construction and Building Materials, V. 17, No. 6-7, 2003, pp. 439-446.
3. Benmokrane, B.; Chaallal, O.; and Masmoudi, R., "Flexural Response of Concrete Beams Reinforced with FRP Reinforcing Bars," ACI Structural Journal, V. 93, No. 1, Jan.-Feb. 1996, pp. 46-55.
4. Masmoudi, R.; Benmokrane, B.; and Chaallal, O., "Cracking Behaviour of Concrete Beams Reinforced with FRP Rebars," Canadian Journal of Civil Engineering, V. 23, No. 6, 1996, pp. 1172-1179.
5. Masmoudi, R.; Thériault, M.; and Benmokrane, B., "Flexural Behavior of Concrete Beams Reinforced with Deformed Fiber Reinforced Plastic Reinforcing Rods," ACI Structural Journal, V. 95, No. 6, Nov.-Dec. 1998, pp. 665-676.
5. Toutanji, H. A., and Saafi, M., "Flexural Behavior of Concrete Beams Reinforced with Glass Fiber-Reinforced Polymer (GFRP) Bars," ACI

Structural Journal, V. 97, No. 5, Nov.-Dec. 1998, pp. 712-719.

6. Thériault, M., and Benmokrane, B., "Effects of FRP Reinforcement Ratio and Concrete Strength on Flexural Behavior of Concrete Beams," *Journal of Composites for Construction*, V. 2, No. 1, 1998, pp. 7-16.

7. Razaqpur, A. G.; Svecova, D.; and Cheung, M. S., "A Rational Method of Deflection Calculation for FRP Reinforced Concrete Beams," *ACI Structural Journal*, V. 97, No. 1, Jan.-Feb. 2000, pp. 175-184.

8. Micelli, F., and Nanni, A., "Durability of FRP Rods for Concrete Structures," *Construction and Building Materials*, V. 18, No. 7, 2004, pp. 491-503.

9. Zollo, R., "Fiber-Reinforced Concrete: An Overview after 30 Years of Development," *Cement and Concrete Composites*, V. 19, No. 2, 1997, pp. 107-122.

10. ACI Committee 544, "Report on Fiber-Reinforced Concrete (ACI 544.1R-96)," American Concrete Institute, Farmington Hills, MI, 1996 (reapproved 2009), 66 pp.

11. Lee, W. K., "Flexural Behavior of Fiber-Reinforced Concrete Beams Reinforced with FRP Bars," master's thesis, Tufts University, Medford, MA, 2003, 161 pp.

12. Jansen, D. C.; Choi, S.; and Shah, S., "Studying Shear Crack Initiation and Growth of Reinforced Concrete Beams Using Full-Field Digital Imaging," *Proceedings of the 2nd International Conference on Nondestructive Testing of Concrete in the Infrastructure*, Nashville, TN, 1996, pp. 195-203.

13. Wang, H., and Belarbi, A., "Flexural Behavior of Fiber-Reinforced-Concrete Beams Reinforced with FRP Rebars," *7th International Symposium on Fiber-Reinforced (FRP) Polymer Reinforcement for Concrete Structures*, SP-230, C. K. Shield, J. P. Busel, S. L. Walkup, and D. D. Gremel, eds., American Concrete Institute, Farmington Hills, MI, 2005, pp. 895-914.

14. ACI Committee 440, "Guide for the Design and Construction of Structural Concrete Reinforced with FRP Bars (ACI 440.1R-06)," American Concrete Institute, Farmington Hills, MI, 2006, 44 pp.

15. Gergely, P., and Lutz, L., "Maximum Crack Width in Reinforced Concrete Flexural Members," *Causes, Mechanisms, and Control of Cracking in Concrete*, SP-20, American Concrete Institute, Farmington Hills, MI, 1968, pp. 87-117.

16. Faza, S. S., and GangaRao, H. V. S., "Theoretical and Experimental Correlation of Behavior of Concrete Beams Reinforced with Fiber Reinforced Plastic Rebars," *Fiber-Reinforced-Plastic Reinforcement for Concrete Structures*, SP-138, A. Nanni and C. W. Dolan, eds., American Concrete Institute, Farmington Hills, MI, 1993, pp. 599-614.

17. Masmoudi, R.; Benmokrane, B.; and Chaalal, O., "Cracking Behavior of Beams Reinforced with FRP Rebars," *First International Conference on Composites in Infrastructures*, H. Saadatmanesh and M. Ehsani, eds., Tucson, AZ, 1996, pp. 374-388.

18. Tighiouart, B.; Benmokrane, B.; and Gao, D., "Investigation on the Bond of Fiber Reinforced Polymer (FRP) Rebars in Concrete," *Second International Conference on Composites in Infrastructures*, V. II, H. Saadatmanesh and M. Ehsani, eds., Tucson, AZ, 1998, pp. 102-112.

19. Masmoudi, R.; Benmokrane, B.; and Chaallal, O., "Cracking Behaviour of Concrete Beams Reinforced with FRP Rebars," *Canadian Journal of Civil Engineering*, V. 23, No. 6, 1996, pp. 1172-1179.

20. Salib, S. R., and Abdel-Sayed, G., "Prediction of Crack Width for Fiber-Reinforced Concrete Beams," *ACI Structural Journal*, V. 101, No. 4, July-Aug. 2004, pp. 532-536.

21. Harajli, M.; Hout, M.; and Jalkh, W., "Local Bond Stress-Slip Behavior of Reinforcing Bars Embedded in Plain and Fiber Concrete," *ACI Materials Journal*, V. 92, No. 4, July-Aug. 1995, pp. 343-354.

22. Harajli, M. H., and Mabsout, M. E., "Evaluation of Bond Strength of Steel Reinforcing Bars in Plain and Fiber-Reinforced Concrete," *ACI Structural Journal*, V. 99, No. 4, July-Aug. 2002, pp. 509-517.

23. Harajli, M.; Hamad, B.; and Karam, K., "Bond-Slip Response of Reinforcing Bars Embedded in Plain and Fiber Concrete," *Journal of Materials in Civil Engineering*, V. 14, No. 6, 2002, pp. 503-511.

24. Malvar, L. J., "Tensile and Bond Properties of GFRP Reinforcing Bars," *ACI Materials Journal*, V. 92, No. 3, May-June 1995, pp. 276-285.

25. Al-Zahrani, M. M.; Al-Dulaijan, S. U.; Nanni, A.; Bakis, C. E.; and Boothby, T. E., "Evaluation of Bond Using FRP Rods with Axisymmetric Deformations," *Construction and Building Materials*, V. 13, No. 6, 1999, pp. 299-309.